Acute Remodeling of Phosphoinositide Lipids Promotes Endocytosis Downstream of RALF/FERONIA Signaling

Nelson B.C. Serre, Marija Smokvarska, Emy Latul, Vincent Bayle, Frédérique Rozier, Claire Lionnet, Vedrana Marković, Mariko Kato, Teun Munnik, Alexandre Martinière, et al.

Title: Acute Remodeling of Phosphoinositide Lipids Promotes Endocytosis Downstream of RALF/FERONIA Signaling

Authors: Nelson BC Serre[1], Marija Smokvarska[2,5], Emy Latul[3], Vincent Bayle[1], Frédérique Rozier[1], Claire Lionnet[1], Vedrana Marković[1], Mariko Kato[4], Teun Munnik[3], Alexandre Martinière[2] and Yvon Jaillais[1].

Affiliations:

1. Laboratoire Reproduction et Développement des Plantes, ENS de Lyon, CNRS, INRAE, Lyon, France
2. IPSiM, Université de Montpellier, CNRS, INRAE, Institut Agro, Montpellier, France
3. Plant Cell Biology, Green Life Sciences Cluster, Swammerdam Institute for Life Sciences, University of Amsterdam, The Netherlands
4. Institute for Chemical Research, Kyoto University, Uji, Kyoto, 611-0011, Japan
5. Present address: Laboratoire de Biogenèse Membranaire, UMR5200, CNRS, Université de Bordeaux, Villenave d'Ornon, France

Lead contact: Yvon Jaillais (yvon.jaillais@ens-lyon.fr)

Keywords: FERONIA, RALF peptide, Receptor-Like Kinase, Microfluidics, Lipid Kinases, Vertical Stage Microscopy, Endocytosis, Membrane Trafficking, Live Imaging, Biosensors

Highlights:

- RALF23 and RALF1 trigger acute PI4P-to-PI(4,5)P_2 conversion at the plasma membrane
- PI(4,5)P_2/PI4P lipid dynamics in response to RALF23 is FERONIA dependent
- PI(4,5)P_2 production in response to RALF23 is controlled by PIP5K7/8/9
- RALF23/FERONIA trigger PI(4,5)P_2 accumulation to promote global endocytosis

Summary:

Phosphoinositides are signaling lipids that regulate cellular responses by acting as gatekeepers of organelle identity or modulating protein localization and activity.[1] They are well established core elements of classical receptor kinase signaling in animals.[2] However, in plants, rapid phosphoinositide remodeling has not yet been recognized as a key regulation of receptor-like kinase signaling.[3,4] Here, we show that the receptor-like kinase FERONIA (FER) triggers acute phosphoinositide remodeling in response to Rapid ALkalinisation Factors23 (RALF23) and RALF1 peptides. Using high-resolution confocal microscopy, combined with microfluidics and advanced image analysis, we reveal that RALF peptides induce a rapid and FER-dependent recruitment of phosphatidylinositol-4,5-bisphosphate (PI(4,5)P_2) sensors at the plasma membrane and a concomitant decrease of phosphatidylinositol-4-phosphate (PI4P) sensors from the cell surface. This PI4P-to-PI(4,5)P_2 conversion is regulated by PI4P 5-Kinase7 (PIP5K7), PIP5K8 and PIP5K9 and is required for RALF-induced endocytosis, a response known to safeguard growth upon recovery from stress episodes.[5–7] These findings highlight a mechanism where FER regulates the PI4P/PI(4,5)P_2 balance through PIP5Ks to control stress-induced endocytosis, linking phosphoinositide dynamics, vesicular trafficking and plant growth adaptation. In addition, it uncovers that peptide/receptor modules have co-opted acute phosphoinositide conversion to act as lipid second messengers in both plant and animal systems.

Results and discussion:

FER is a transmembrane receptor-like kinase involved in response to stresses, developmental signaling events, innate immunity and reproduction.[8–11] Its extracellular domain binds RALF peptides, which triggers pleiotropic rapid extracellular and intracellular responses, such as cell wall alkalinization, global endocytosis, calcium influx and ROS accumulation.[8–11] Recently, Smokvarska et al., 2023 linked RALF/FER and anionic phospholipids signaling by demonstrating that the plasma membrane phosphatidylserine content was rapidly but transiently increased at the plasma membrane in response to RALF23.[12] Phosphatidylserine is an anionic lipid required for the nano-organization of the Rho GTPase ROP6 at the plasma membrane and its downstream signaling.[13] Thus, the regulation of phosphatidylserine accumulation at the plasma membrane by RALF23/FER tunes Rho GTPase signaling in plants.[12–15] Here, we set out to analyze whether RALF/FER signaling may regulate the dynamics of other anionic phospholipids at the plasma membrane, notably the phosphoinositides, PI4P and PI(4,5)P_2, and what could be the underlying mechanism. Despite their relatively low abundances, these lipids play key roles in plant development and stress responses.[16,17] Because RALFs induce rapid and transient responses, including the regulation of phosphatidylserine subcellular accumulation patterns, we decided to use a microfluidic setup (**Figure S1A,B**). This strategy enables to follow the localization of fluorescent molecules by live imaging before and after injection of the RALF peptide.[18–20] To follow lipid dynamics, we used transgenic lines stably expressing fluorescent lipid reporters.[21,22] Theses so called lipid biosensors consist of a protein domain that specifically binds to a given lipid, fused to a fluorescent protein. As such, they are made in the cytosol and they are targeted to specific membranes via their interaction with their cognate lipid, thereby indirectly reporting on the localization of this lipid. To quantify the degree of recruitment of each sensor at the plasma membrane, we compiled their association index: the ratio of fluorescence between signal at the plasma membrane and the intracellular space in the treated condition over a similar ratio obtained in the control condition (**Figure 1A**).[12,13,23–25] We then developed an imaging method and the associated semi-automated image analysis pipeline to process raw microscope movies into association index (**Figure S1C**). Seedlings expressing a biosensor of interest were imaged on a vertical stage confocal microscope every two minutes in microfluidics at several z planes (over 7 microns in depth) allowing the registration of every movie in 5 dimensions (x,y,z coordinates, time and 2 color channels, see methods for details and **Figure 1B, S1C**).

To validate our analysis pipeline, we first imaged the mCITRINE-2PH(EVECTIN2) phosphatidylserine sensor.[12,26] In response to 5 µM RALF23, the phosphatidylserine reporter accumulated transiently at the plasma membrane, with a peak at 15 minutes (**Figure 1C,D**). This dynamic closely mirror the published results obtained with end-point assays and manual quantification.[12] Furthermore, a switch from control medium to control medium did not influence the biosensor localization or its intensity (**Figure 1C,D**), further validating our microfluidics set-up and image analysis pipeline. Finally, we also showed that the transient accumulation of the phosphatidylserine biosensor at the plasma membrane was RALF23-concentration dependent and was saturating above 3 µM (**Figure S1D**).

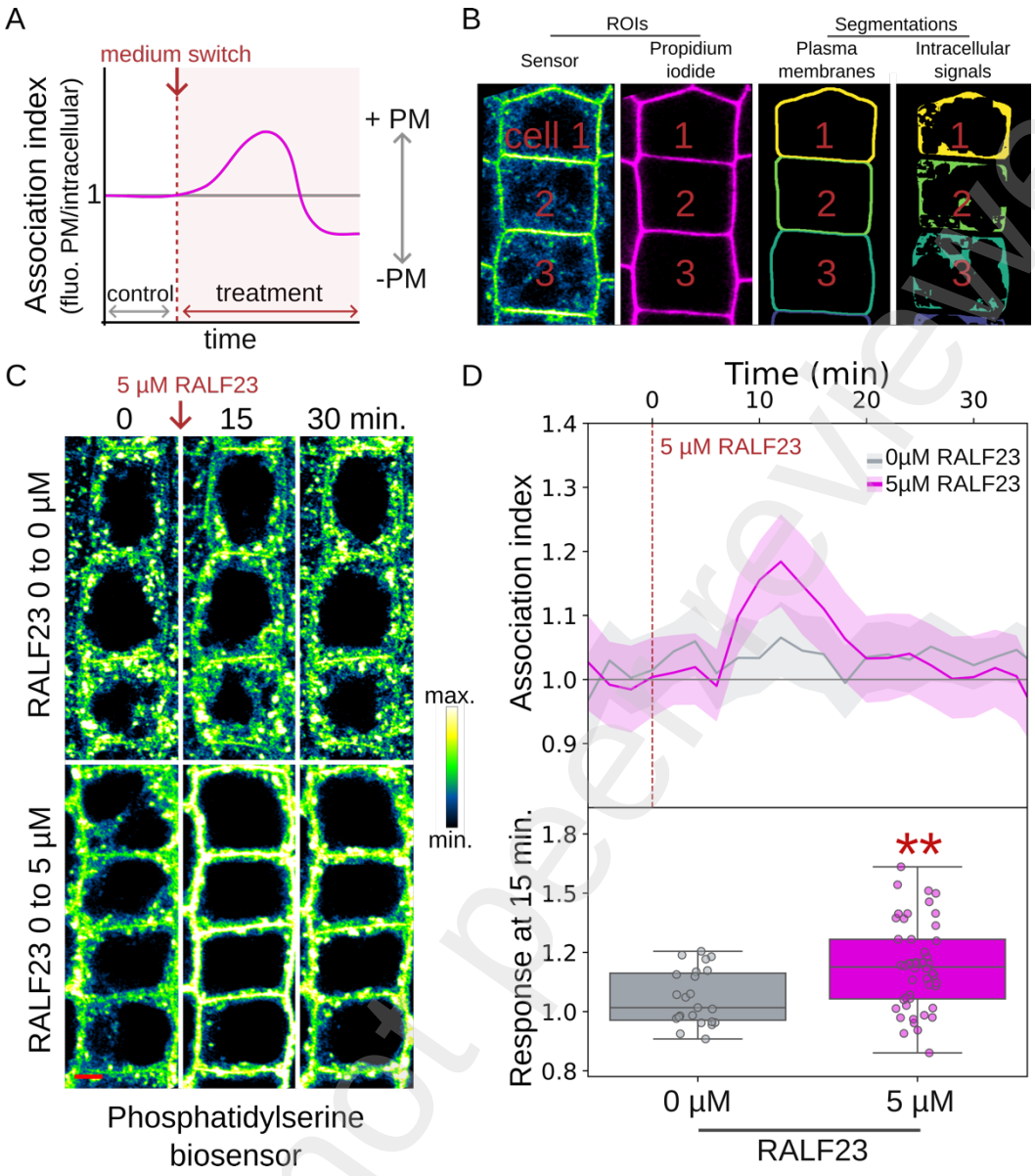

Figure 1: Development and validation of an image analysis pipeline to quantify lipid sensor subcellular dynamics. ***A****) Schematic representation of a graphic representing the association index (Fluorescence PM/intra) over time. Note that here and throughout the following figures, the dotted vertical red line indicates when the seedlings were treated and the gray horizontal line indicates a ratio of 1 for visual reference. An association index above 1 indicates that the fluorescent reporter is recruited to the plasma membrane (+PM), while an association index below 1, indicates that the fluorescent reporter dissociates from the plasma membrane (-PM).* ***B****) Example of manually selected region of interest (ROIs) and their plasma membrane and intracellular signal segmentation from our automatic image segmentation pipeline. Original image from mCITRINE-2PH(EVECTIN2).* ***C****) Representative microscopy images of the phosphatidylserine biosensor mCITRINE-2PH(EVECTIN2) imaged in microfluidic. Seedlings were imaged in control condition (t0) and then in treatment condition 0 or 5 µM RALF23 (t15 and t30). Scale bar = 5µm.* ***D****) Upper panel: Quantification of the mCITRINE-2PH(EVECTIN2) association index over time (minutes). Lower panel: Box plots showing the distribution of association index values in individual cells at 15 minutes, for control (0 µM RALF23) and treated (5 µM RALF23) conditions. n cells [23-48] from [8-11] individual seedlings. p-value = 0.0048 (p < 0.01: **). See also Figure S1.*

Next, we analyzed the localization of mCITRINE-1PH(FAPP1)[27], a PI4P sensor, in response to 5 µM of RALF23. We found a strong depletion of the plasma membrane pool of this PI4P reporter within the first minutes of treatment before stabilizing after 15 minutes. The relocalization was evidenced by both the loss of plasma membrane signal and a rapid accumulation of fluorescent intracellular compartments (**Figure 2A,B and video S1**). PI4P in plants was previously shown to accumulate at the plasma membrane and to a lesser extent in endosomes.[24,26–28] The localization of PI4P sensors reflect this balance, with a strong accumulation in the plasma membrane and little to no signal in intracellular compartments in resting conditions.[24,29] It is thus likely that RALF23 treatment decreases PI4P levels at the plasma membrane, skewing the localization of the PI4P sensor toward endosomes (**Figure 2A,B**). However, we cannot exclude that PI4P levels are instead increased in endosomes, which would also enhance the localization of the PI4P sensor toward this compartment. In either case, like for phosphatidylserine, PI4P dynamics upon RALF23 treatment was dose dependent (**Figure S2A,B**). Furthermore, this response was confirmed with another PI4P biosensor, mCITRINE-1PH(OSBP),[27] which displayed a similar dynamics than mCITRINE-1PH(FAPP1) following RALF23 treatment (**Figure S2C,D and video S1**).

We also quantified the dynamics of $PI(4,5)P_2$ in response to RALF23 using the high affinity biosensor mCITRINE-2PH(PLC)[27]. We found that this sensor strongly accumulated at the plasma membrane as early as 2-to-4 minutes after RALF23 treatment before reaching a plateau at approximately 15 minutes (**Figure 2C,D and video S2**). Accumulation at the plasma membrane was accompanied by a strong decrease in cytosolic signal. Again, this response was dose-dependent (**Figure S2E,F**) and validated with two additional $PI(4,5)P_2$ biosensor, mCITRINE-1PH(PLC) and mCITRINE-1TUBBYc (**Figure S2G,H and video S2**). It is worth noting that each biosensor has a different basal subcellular fluorescence, especially in the amount of cytosolic signal present in the control condition. This is explained by the respective affinities of these biosensors for $PI(4,5)P_2$.[27] Indeed, mCITRINE-2PH(PLC) is a high-affinity sensor, which localizes at the plasma membrane in the absence of stimulation even when $PI(4,5)P_2$ levels at the plasma membrane are very low.[27] By contrast, mCITRINE-1PH(PLC) is a low-affinity sensor, which accumulates mainly in the cytosol and is only recruited to the plasma membrane upon $PI(4,5)P_2$ production.[30–32] In this context, while the three biosensors were rapidly recruited at the plasma membrane upon RALF23 treatment, the strength of the response was different, with increasing responses from mCITRINE-2PH(PLC), to mCITRINE-1TUBBYc and mCITRINE-1PH(PLC). Altogether, our results suggest that RALF23 treatment rapidly induces phosphoinositide remodeling at the plasma membrane, with decreased PI4P levels accompanied by increased $PI(4,5)P_2$ levels.

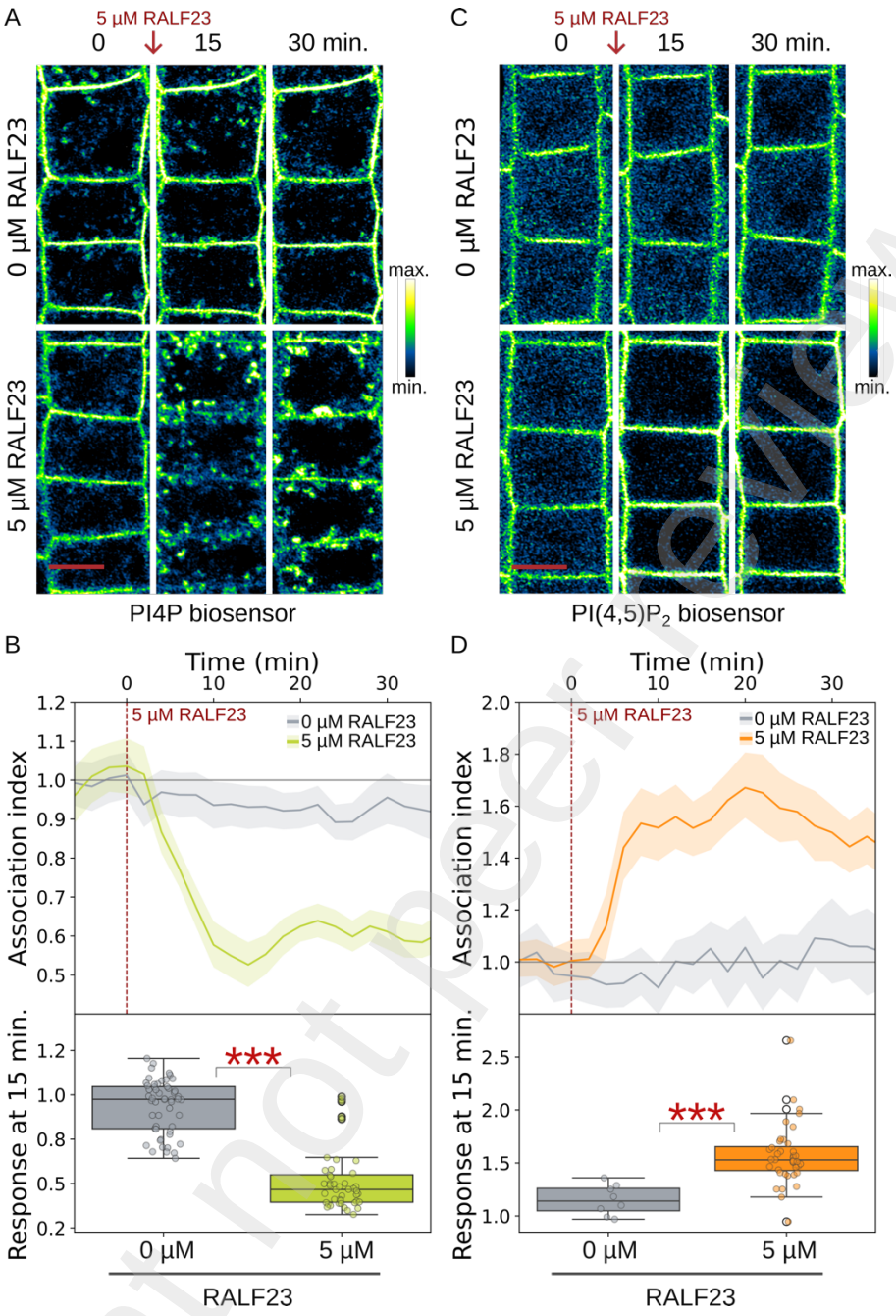

Figure 2: RALF23 acutely impacts the subcellular localization of PI4P and PI(4,5)P₂ in the root. ***A,C****) Representative microscopy images of A) PI4P biosensor mCITRINE-1PH(FAPP1) and B) PI(4,5)P₂ biosensor mCITRINE-2PH(PLC) imaged in microfluidic. Seedlings were imaged in control condition (t0) and then in treatment condition 0 or 5 µM RALF23 (t15 and t30). Scale bar = 10 µm.* ***B,D****) Upper panel: Quantification of the B) mCITRINE-1PH(FAPP1) and D) mCITRINE-2PH(PLC) association index over time (minutes). Lower panel: Box plots showing the distribution of association index values in individual cells at 15 minutes, for control (0 µM RALF23) and treated (5 µM RALF23) conditions. For B) n cells [44-52] from [8-9] individual seedlings. p-value = $2.81e^{-14}$ ($p < 0.001$: ***). and D) n cells [8-40] from [4-8] individual seedlings . p-value = $6.96e^{-06}$($p < 0.001$: ***). See also Figure S2 and Video S1 and S2.*

RALF peptides are known to act as ligands for receptor-like kinases from the *Catharanthus roseus* receptor-like kinase 1-like (CrRLK1L) protein subfamily, including FER.[33,34] RALF1 and RALF23 are both known to bind to and activate FER[35–38]. We found that the dynamic relocalizations of the PI4P and PI(4,5)P_2 biosensors triggered upon RALF23 treatment, were also observed when applying the RALF1 peptide (**Figure 3A**), suggesting that FER could be the receptor involved in the lipid remodeling response. To test this hypothesis, we generated generated f*er* knock-out mutants using CRISPR-Cas0 in mCITRINE-1PH(FAPP1) and mCITRINE-2PH(PLC) expressing lines (**Figure S3**). RALF23 failed to induce any dynamic relocalization of the PI4P (**Figure 3B,C**) and PI(4,5)P_2 biosensors in *fer* mutants (**Figure 3D,E**). Thus, FER is essential for the opposite PI4P/PI(4,5)P_2 dynamics to take place in response to RALF23.

When comparing the association of PI4P and PI(4,5)P_2 biosensors with the plasma membrane during RALF23 treatment, we noticed that these responses showed an almost perfectly mirrored dynamics over time, being visible 2-to-4 minutes following RALF23 treatment and with a peak of response between 10 and 15 minutes post-treatment (**Figure 4A**). These dynamics are compatible with a scenario in which PI4P is converted at the plasma membrane into PI(4,5)P_2, thereby leading to the recruitment of PI(4,5)P_2 biosensors and the reduction of PI4P reporter at the cell surface. Such interconversion could indicate an activation of PI4P 5-kinases (PIP5K) at the plasma membrane upon RALF treatment (**Figure 4B**). To test this hypothesis, we investigated the role of the PIP5Ks: PIP5K7, PIP5K8 and PIP5K9 (hereafter PIP5K7/8/9). These three PIP5Ks are involved in regulating PI(4,5)P_2 content in response to NaCl, osmotic stress and polyamine.[30,39] This stresses overlap with the known function of FER in stress signaling.[7,33,40] Upon RALF23 treatment, the accumulation of PI(4,5)P_2 at the plasma membrane was critically impaired in both the double *pip5k7,9* and triple *pip5k7,8,9* mutants indicating that PIP5K7/8/9 isoforms are major actors regulated by RALF23 and FER to modulate the plasma membrane pool of PI(4,5)P_2 through phosphorylation of PI4P (**Figure 4C, D and video S3**).

To further determine the link between FER and PIP5Ks, we explored PIP5K7, 8 and 9 localizations. Mannitol treatment was shown to trigger the relocalization of PIP5K8 and PIP5K9 into intracellular compartments.[39] We thus analyzed whether RALF23 treatment similarly impacted the subcellular localization of these three PIP5Ks. Using our microfluidic and quantification pipeline, we found that RALF23 did not impact the subcellular localization of PIP5K7-YFP, PIP5K8-YFP and PIP5K9-YFP. Each PIP5K-YFP isoform strictly localized at the plasma membrane independently of the presence of RALF23 (**Figure S4A,B**). During the course of PIP5K imaging, we noticed that PIP5K7-YFP was organized in nanodomains at the plasma membrane (**Figure S4C**).[41] Such organization in nanodomains was previously reported for other lipid kinases, including the PI4Kinase alpha1 and the PIP5K2 isoforms.[42,43] Addition of RALF23 for 15 minutes did not produce any significant effects on PIP5K7-YFP cluster density and size at the plasma membrane (**Figure S4C-D**). Thus, it is likely that RALF23/FER signaling regulates PIP5K7/8/9 activity rather than their subcellular targeting. Furthermore, the strict constitutive plasma membrane localization of PIP5K7/8/9 confirms that the phosphoinositide remodeling happens at the cell surface rather than in endosomes.

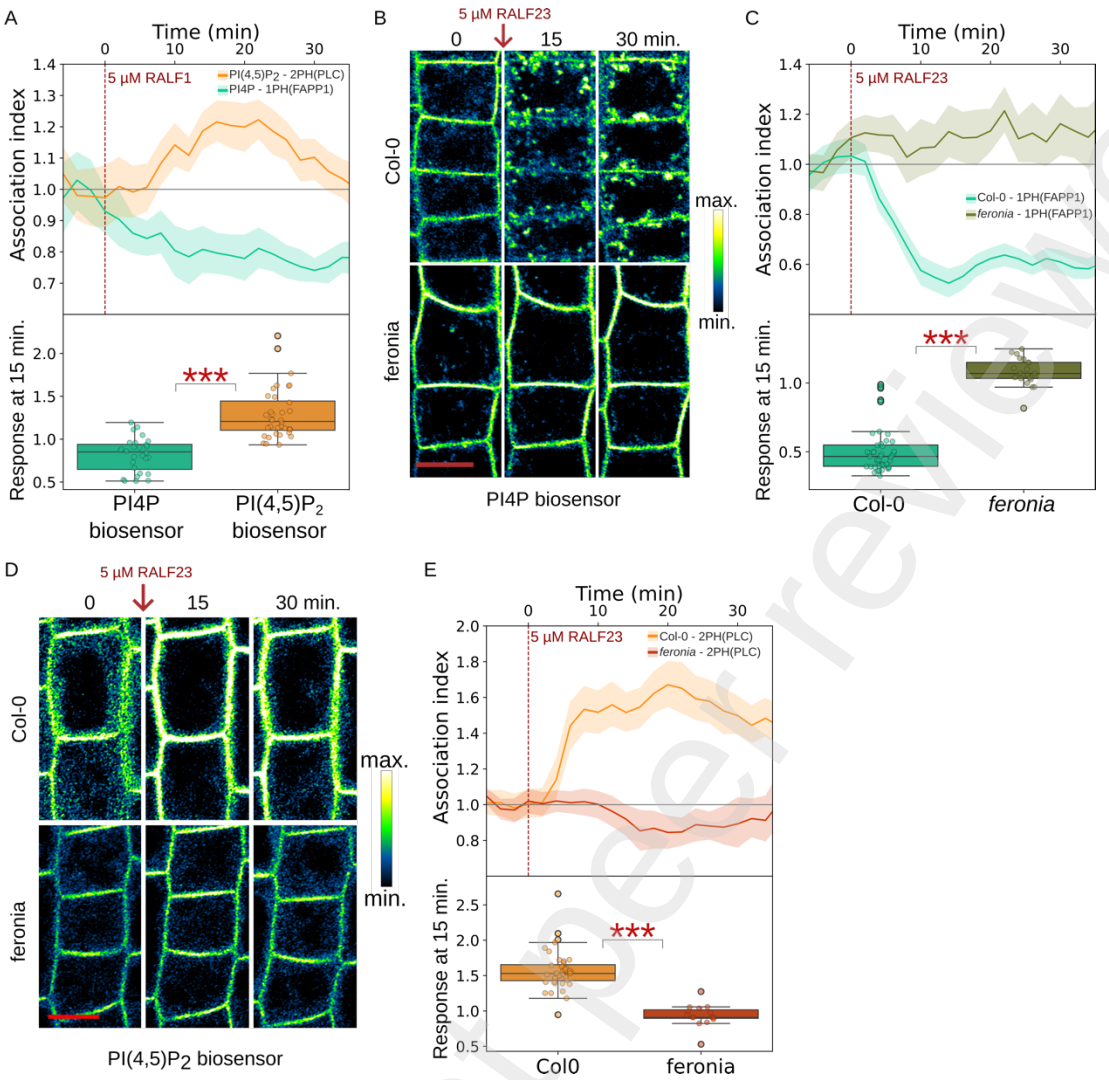

Figure 3: PI4P and PI(4,5)P₂ dynamics in response to RALF23 are dependent on the receptor-like kinase FERONIA. A*) Upper panel: Quantification of the mCITRINE-1PH(FAPP1) and mCITRINE-2PH(PLC) association index over time (minutes). Seedlings were imaged in control condition (t0) and then in treatment condition with 5 µM RALF1 (t15 and t30). Lower panel: Box plots showing the distribution of association index values in individual cells at 15 minutes. n cells [28-36] from [6-7] individual seedlings. p-value = 4.16e^{-15} (p < 0.001: ***).* ***B,D****) Representative microscopy images of B) PI4P biosensor mCITRINE-1PH(FAPP1) in Col-0 or feronia backgrounds and D) PI(4,5)P₂ biosensor mCITRINE-2PH(PLC) in Col-0 or feronia background imaged in microfluidic. Seedlings were imaged in control condition (t0) and then in treatment condition with 5 µM RALF23 (t15 and t30). Scale bar = 10 µm. C,E) Upper panel: Quantification of the C) mCITRINE-1PH(FAPP1) and E) mCITRINE-2PH(PLC) association index over time (minutes) in both Col-0 and feronia backgrounds. Lower panel: Box plots showing the distribution of association index values in individual cells at 15 minutes treated with 5 µM RALF23. For C) n cells [21-44] from [8] individual seedlings, p-value = 2.19e^{-10} (p < 0.001: ***). and E) n cells [15-40] from [4-8] individual seedlings, p-value = 4.02e^{-08} (p < 0.001: ***). Note that the data for the mCITRINE-1PH(FAPP1) and mCITRINE-2PH(PLC) in Col-0 background in RALF23 5 µM condition are the same as in figure 2. See also Figure S3.*

RALF1 and RALF23 peptides and their receptor FER are known to enhance the endocytosis process in a global manner, including the internalization of FER itself, to regulate root growth and development.[6,44,45] Furthermore, it was recently reported that RALF1 and pectins act as surface sensors, reacting to stress by phase separation, which triggers FER clustering and induces bulk endocytosis of many membrane proteins.[7] Given that PI(4,5)P_2 is a key positive regulator of endocytosis,[46–48] we investigated if the phospholipid dynamics described above could have a role in the RALF-induced endocytosis. To do so, we performed FM4-64 internalization assays,[49] in the wild type Col-0 and the triple *pip5k*7,8,9 mutant. Col-0 cells displayed a higher percentage of cells with tonoplast staining (**Figure 4E,F**) and larger intracellular FM4-64-labelled compartments (**Figure S4F**) after 15 minutes of RALF23 treatments, than in the mock conditions. This quantification indicated a stronger or faster endocytic fluxes after RALF23 treatment, which confirmed previous reports.[6,7] In *pip5k7,8,9*, the percentage of cells with tonoplast staining and the size of FM4-64-labelled endosomes remained low in the presence or absence of RALF23 (**Figure 4E,F**), indicating that PIP5K7/8/9 are essential for the global stimulation of endocytosis triggered by RALF23. To confirm the role of PIP5Ks in the stimulation of the endocytic process in response to RALF23, we next analyzed the endocytosis of PIN2-GFP, a known cargo protein internalized upon RALF treatment.[6,7] As reported for RALF1, we found that RALF23 treatment triggered the internalization of PIN2-GFP into intracellular compartments (**Figure 4G-H**). We next introduced PIN2-GFP in the *pip5k7,8,9* triple mutant, and found that PIN2-GFP endocytosis was not boosted by RALF23 in this mutant and remained at a similar level in the presence or absence of RALF23 treatment (**Figure 4G-H**). Taken together, we concluded from these experiments that PIP5K7/8/9 are required for both the rapid PI(4,5)P_2 production at the plasma membrane and the global increase of endocytic activity triggered by RALF treatment.

Concluding remarks:

Here, we found that RALF peptides trigger an acute phosphoinositide remodeling by promoting a PI4P-to-PI(4,5)P_2 conversion at the plasma membrane. One function of this rapid lipid remodeling is to increase the global levels of endocytosis, which is involved in growth recovery after abiotic stresses.[7] In line with FER pleotropic functions, it is likely that PI(4,5)P_2 acute synthesis at the plasma membrane controls additional cellular pathways. For example, the C2 domain ABA-related (CAR) proteins, are known effectors of anionic phospholipids and are recruited at the plasma membrane upon RALF1 treatment.[50]

PI(4,5)P_2 production is inhibited upon the perception of the flagellin-derived peptide flg22 by its receptor kinase FLAGELIN INSENSITIVE2 (FLS2).[51] Flg22 triggers the activation of MITOGEN-ACTIVATED PROTEIN KINASE6 (MPK6), which in turn phosphorylates and inactivates PIP5K6, thereby downregulating the levels of PI(4,5)P_2. Consistent with our findings, reduction of PI(4,5)P_2 synthesis upon flg22 treatment inhibits global endocytosis.[51] Thus, flg22 and RALF peptides act via different PIP5K isoforms to mediate opposite effects on PI(4,5)P_2 levels and global endocytic fluxes. PIP5K6 is inhibited by phosphorylation upon flg22 treatment,[51] while it remains to be determined how PIP5K7/8/9 are activated by the RALF/FER pathway. Although flg22-triggered PI(4,5)P_2 inhibition was measured at late time points (60-to-90 minutes post flg22 treatment),[51] the global modulation of endocytosis appears as a major cellular target controlled by phosphoinositides downstream of plant receptor kinases. Furthermore, our work establishes that phosphoinositide conversion can be an acute response downstream of receptor kinases in plants, which is reminiscent of classical signaling pathways in animals.

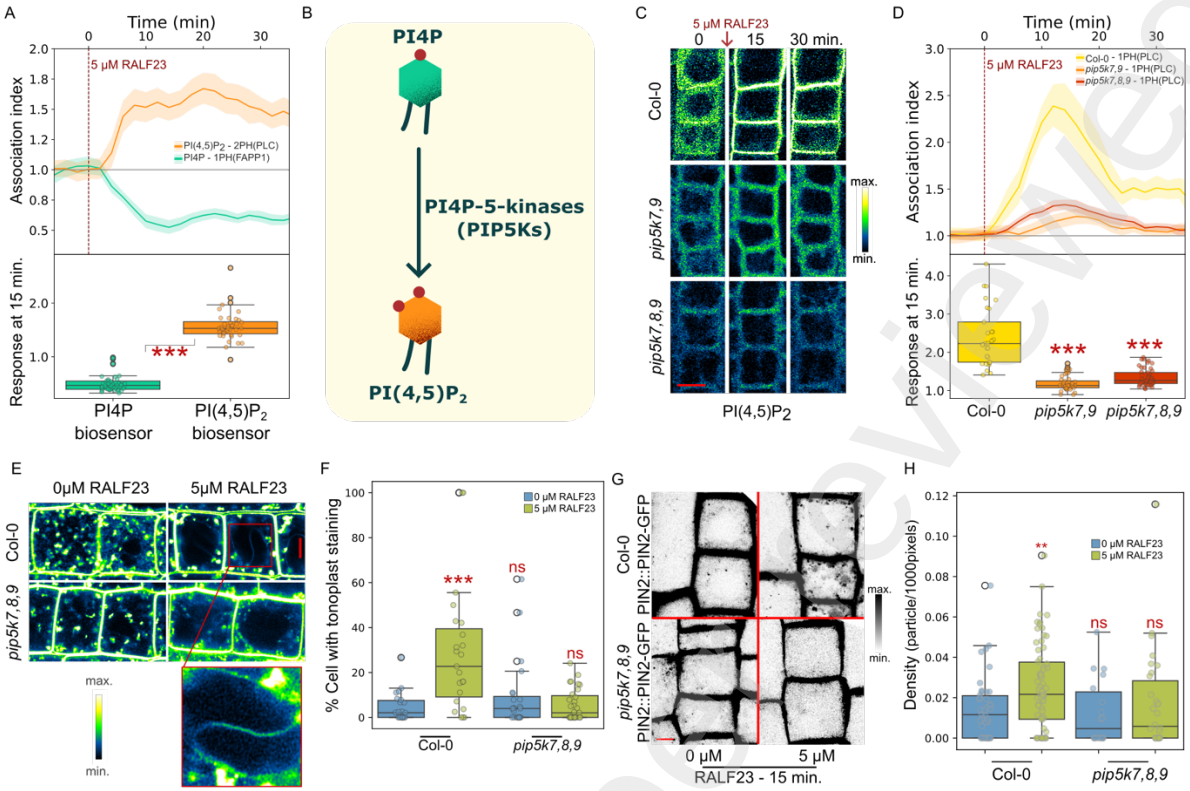

Figure 4: PI(4,5)P₂ production in response to RALF23 is produced by PIP5K7/8/9 and required for general endocytosis. ***A)*** *Upper panel: Quantification of the mCITRINE-1PH(FAPP1) and mCITRINE-2PH(PLC) association index over time (minutes) in response to 5 µM RALF23. Lower panel: Box plots showing the distribution of association index values in individual cells at 15 minutes treated with 5 µM RALF23. n cells [40-44] from [8] individual seedlings. P-value: 4.16e^{-15} (p < 0.001: ***).* ***B)*** *Schematic representation of PI4P-to-PI(4,5)P2 conversion by PIP5Ks.* ***C)*** *Representative microscopy images of PI(4,5)P₂ biosensor mCITRINE-1PH(PLC) in Col-0 and pip5k7,8,9 backgrounds imaged in microfluidic. Seedlings were imaged in control condition (t0) and then in treatment condition with 5 µM RALF23 (t15 and t30). Scale bar = 10 µm.* ***D)*** *Upper panel: Quantification of the association index over time (minutes) of mCITRINE-1PH(PLC) in Col-0, pip5k7,9 and pip5k7,8,9 backgrounds in response to 5 µM RALF23. Lower panel: Box plots showing the distribution of association index values in individual cells at 15 minutes treated with 5 µM RALF23. n cells [29-48] from [5-10] individual seedlings. p-value= Col-0 vs pip5k7,9: 1.03e^{-11} and Col-0 vs pip5k7,8,9: 3.39e^{-11} (p < 0.001: ***).* ***E)*** *Representative microscopy images of Col-0 and pip5k7,8,9 mutant after FM4-64 internalization assays. Seedlings were imaged after 15 to 20 minutes treatment with 0 or 5 µM RALF23. Scale bar = 5 µm.* ***F)*** *Quantification of the percentage of cells presenting tonoplast staining per seedling. [22-31] individual seedlings. p-values are detailed in Supplementary file (p>0,05: non significant (ns), p < 0.001: ***).* ***G)*** *Representative microscopy images of PIN2::PIN2-GFP in Col-0 and pip5k7,8,9 backgrounds imaged after 15 to 20 minutes treatment with 5 µM RALF23. Scale bar = 5 µm.* ***H)*** *Quantification of intracellular particle density for 1000 pixels of PIN2::PIN2-GFP in Col-0 and pip5k7,8,9 backgrounds after 15 minutes treatment with 5 µM RALF23. [19-79] individual seedlings. p-values are detailed in Supplementary file (p > 0.05: non significant (ns), p < 0.01: **). See also Figure S4 and Video S3.*

Acknowledgements:
We thank Stéphane Guillet and Denis Bartolo (Physics laboratory, ENS de Lyon) for kindly teaching us the UV-Photolithography process, the SiCE group for discussion, comments, and technical help. This project has received funding from the European Research Council (ERC) under the European Union's Horizon 2020 research and innovation program (Grant Agreement No 101001097) and by an EMBO Long-Term Fellowship to V.M. ALTF 466-2022.

Author contributions:
Preliminary data, MS, VM, AM, MK; Conceptualization, YJ, AM and NBCS; Methodology, YJ, NBCS, VB and CL; Investigation, Data analysis, programming and graphics, NBCS; Original draft, YJ and NBCS; Review and editing, All authors; Funding acquisition, YJ; Supervision, YJ.

Declaration of interests:
The authors declare no competing interests.

References:
1. Posor, Y., Jang, W., and Haucke, V. (2022). Phosphoinositides as membrane organizers. Nat Rev Mol Cell Biol *23*, 797–816. https://doi.org/10.1038/s41580-022-00490-x.
2. Lodish, H.F., Berk, A.J., and Kaiser, C.A. (2016). Molecular cell biology Eighth edition. (New York : W. H. Freeman and Company).
3. Heilmann, M., and Heilmann, I. (2022). Regulators regulated: Different layers of control for plasma membrane phosphoinositides in plants. Current Opinion in Plant Biology *67*, 102218. https://doi.org/10.1016/j.pbi.2022.102218.
4. Noack, L.C., and Jaillais, Y. (2020). Functions of Anionic Lipids in Plants. Annual Review of Plant Biology *71*, 71–102.
5. Xing, J., Ji, D., Duan, Z., Chen, T., and Luo, X. (2022). Spatiotemporal dynamics of FERONIA reveal alternative endocytic pathways in response to flg22 elicitor stimuli. New Phytologist *235*, 518–532. https://doi.org/10.1111/nph.18127.
6. Yu, M., Li, R., Cui, Y., Chen, W., Li, B., Zhang, X., Bu, Y., Cao, Y., Xing, J., Jewaria, P.K., et al. (2020). The RALF1-FERONIA interaction modulates endocytosis to mediate control of root growth in *Arabidopsis*. Development, dev.189902. https://doi.org/10.1242/dev.189902.
7. Liu, M.-C.J., Yeh, F.-L.J., Yvon, R., Simpson, K., Jordan, S., Chambers, J., Wu, H.-M., and Cheung, A.Y. (2024). Extracellular pectin-RALF phase separation mediates FERONIA global signaling function. Cell *187*, 312-330.e22. https://doi.org/10.1016/j.cell.2023.11.038.
8. Tang, J., and Guo, H. (2025). Jack of all trades: crosstalk between FERONIA signaling and hormone pathways. Journal of Experimental Botany *76*, 1907–1920. https://doi.org/10.1093/jxb/eraf071.
9. Zhu, S., Fu, Q., Xu, F., Zheng, H., and Yu, F. (2021). New paradigms in cell adaptation: decades of discoveries on the CrRLK1L receptor kinase signalling network. New Phytologist *232*, 1168–1183. https://doi.org/10.1111/nph.17683.
10. Lin, Z., Liu, D., Xu, Y., Wang, M., Yu, Y., Diener, A.C., and Liu, K. (2024). Pupylation-based proximity-tagging of FERONIA-interacting proteins in Arabidopsis. Molecular & Cellular Proteomics, 100828. https://doi.org/10.1016/j.mcpro.2024.100828.
11. Malivert, A., and Hamant, O. (2023). Why is FERONIA pleiotropic? Nat. Plants, 1–8. https://doi.org/10.1038/s41477-023-01434-9.

12. Smokvarska, M., Bayle, V., Maneta-Peyret, L., Fouillen, L., Poitout, A., Dongois, A., Fiche, J.-B., Gronnier, J., Garcia, J., Höfte, H., et al. (2023). The receptor kinase FERONIA regulates phosphatidylserine localization at the cell surface to modulate ROP signaling. Sci Adv *9*, eadd4791. https://doi.org/10.1126/sciadv.add4791.
13. Platre, M.P., Bayle, V., Armengot, L., Bareille, J., Marquès-Bueno, M.D.M., Creff, A., Maneta-Peyret, L., Fiche, J.-B., Nöllmann, M., Miège, C., et al. (2019). Developmental control of plant Rho GTPase nano-organization by the lipid phosphatidylserine. Science (New York, NY) *364*, 57–62.
14. Smokvarska, M., Francis, C., Platre, M.P., Fiche, J.-B., Alcon, C., Dumont, X., Nacry, P., Bayle, V., Nöllmann, M., Maurel, C., et al. (2020). A Plasma Membrane Nanodomain Ensures Signal Specificity during Osmotic Signaling in Plants. Current Biology, 1–26.
15. Boutté, Y., and Jaillais, Y. (2020). Metabolic Cellular Communications: Feedback Mechanisms between Membrane Lipid Homeostasis and Plant Development. Developmental Cell, 1–12.
16. Heilmann, M., and Heilmann, I. (2025). Getting attached to membranes—How plant signaling networks employ PtdIns(4,5)P2. Plant Physiology *197*. https://doi.org/10.1093/plphys/kiae393.
17. Marković, V., and Jaillais, Y. (2022). Phosphatidylinositol 4-phosphate: a key determinant of plasma membrane identity and function in plants. New Phytologist *235*, 867–874. https://doi.org/10.1111/nph.18258.
18. Li, L., Chen, H., Alotaibi, S.S., Pěnčík, A., Adamowski, M., Novák, O., and Friml, J. (2022). RALF1 peptide triggers biphasic root growth inhibition upstream of auxin biosynthesis. Proc Natl Acad Sci U S A *119*, e2121058119. https://doi.org/10.1073/pnas.2121058119.
19. Serre, N.B.C., k, D.K. x000ED, Yun, P., Slouka, Z. x0011B k, Shabala, S., and Fendrych, M. x000E1 amp x00161 (2021). AFB1 controls rapid auxin signalling through membrane depolarization in Arabidopsis thaliana root. Nature Plants, 1–12.
20. Grossmann, G., Guo, W.J., Ehrhardt, D.W., Frommer, W.B., Sit, R.V., Quake, S.R., and Meier, M. (2012). The RootChip: An Integrated Microfluidic Chip for Plant Science. THE PLANT CELL ONLINE *23*, 4234–4240.
21. Colin, L., Martin-Arevalillo, R., Bovio, S., Bauer, A., Vernoux, T., Caillaud, M.-C., Landrein, B., and Jaillais, Y. (2021). Imaging the living plant cell: from probes to quantification. THE PLANT CELL ONLINE.
22. de Jong, F., and Munnik, T. (2021). Attracted to Membranes: Lipid-Binding Domains in Plants. PLANT PHYSIOLOGY.
23. Hammond, G.R.V., Fischer, M.J., Anderson, K.E., Holdich, J., Koteci, A., Balla, T., and Irvine, R.F. (2012). PI4P and PI(4,5)P2 are essential but independent lipid determinants of membrane identity. Science (New York, NY) *337*, 727–730.
24. Simon, M.L.A., Platre, M.P., Marquès-Bueno, M.M., Armengot, L., Stanislas, T., Bayle, V., Caillaud, M.-C., and Jaillais, Y. (2016). A PtdIns(4)P-driven electrostatic field controls cell membrane identity and signalling in plants. Nature Plants, 1–10.
25. Marquès-Bueno, M.M., Armengot, L., Noack, L.C., Bareille, J., Rodriguez, L., Platre, M.P., Bayle, V., Liu, M., Opdenacker, D., Vanneste, S., et al. (2021). Auxin-Regulated Reversible Inhibition of TMK1 Signaling by MAKR2 Modulates the Dynamics of Root Gravitropism. Current Biology *31*, 228-237.e10. https://doi.org/10.1016/j.cub.2020.10.011.
26. Platre, M.P., Noack, L.C., Doumane, M., Bayle, V., Simon, M.L.A., Maneta-Peyret, L., Fouillen, L., Stanislas, T., Armengot, L., Pejchar, P., et al. (2018). A Combinatorial Lipid

Code Shapes the Electrostatic Landscape of Plant Endomembranes. Developmental Cell, 1–28.
27. Simon, M.L.A., Platre, M.P., Assil, S., van Wijk, R., Chen, W.Y., Chory, J., Dreux, M., Munnik, T., and Jaillais, Y. (2013). A multi-colour/multi-affinity marker set to visualize phosphoinositide dynamics in Arabidopsis. The Plant journal : for cell and molecular biology, n/a-n/a.
28. Vermeer, J.E.M., Thole, J.M., Goedhart, J., Nielsen, E., Munnik, T., and Gadella, T.W.J. (2009). Imaging phosphatidylinositol 4-phosphate dynamics in living plant cells. The Plant journal : for cell and molecular biology *57*, 356–372.
29. Ito, Y., Esnay, N., Platre, M.P., Wattelet-Boyer, V., Noack, L.C., Fougère, L., Menzel, W., Claverol, S., Fouillen, L., Moreau, P., et al. (2021). Sphingolipids mediate polar sorting of PIN2 through phosphoinositide consumption at the trans-Golgi network. Nat Commun *12*, 4267. https://doi.org/10.1038/s41467-021-24548-0.
30. Zarza, X., van Wijk, R., Shabala, L., Hunkeler, A., Lefebvre, M., Rodriguez-Villalon, A., Shabala, S., Tiburcio, A.F., Heilmann, I., and Munnik, T. (2020). Lipid kinases PIP5K7 and PIP5K9 are required for polyamine-triggered K +efflux in Arabidopsis roots. The Plant journal : for cell and molecular biology, tpj.14932.
31. Mishkind, M., Vermeer, J.E.M., Darwish, E., and Munnik, T. (2009). Heat stress activates phospholipase D and triggers PIP2 accumulation at the plasma membrane and nucleus. The Plant Journal *60*, 10–21. https://doi.org/10.1111/j.1365-313X.2009.03933.x.
32. van Leeuwen, W., Vermeer, J.E.M., Gadella, T.W.J., and Munnik, T. (2007). Visualization of phosphatidylinositol 4,5-bisphosphate in the plasma membrane of suspension-cultured tobacco BY-2 cells and whole Arabidopsis seedlings. The Plant journal : for cell and molecular biology *52*, 1014–1026.
33. Cheung, A.Y. (2024). FERONIA: A Receptor Kinase at the Core of a Global Signaling Network. Annual Review of Plant Biology *75*, 345–375. https://doi.org/10.1146/annurev-arplant-102820-103424.
34. Schoenaers, S., and Vissenberg, K. (2025). Overlooked aspects of CrRLK1L–RALF signaling. New Phytologist *n/a*. https://doi.org/10.1111/nph.70422.
35. Abarca, A., Franck, C.M., and Zipfel, C. (2021). Family-wide evaluation of RAPID ALKALINIZATION FACTOR peptides. Plant Physiol *187*, 996–1010. https://doi.org/10.1093/plphys/kiab308.
36. Stegmann, M., Monaghan, J., Smakowska-Luzan, E., Rovenich, H., Lehner, A., Holton, N., Belkhadir, Y., and Zipfel, C. (2017). The receptor kinase FER is a RALF-regulated scaffold controlling plant immune signaling. Science (New York, NY) *355*, 287–289.
37. Blackburn, M.R., Haruta, M., and Moura, D.S. (2020). Twenty Years of Progress in Physiological and Biochemical Investigation of RALF Peptides. PLANT PHYSIOLOGY *182*, 1657–1666.
38. Haruta, M., Sabat, G., Stecker, K., Minkoff, B.B., and Sussman, M.R. (2014). A Peptide Hormone and Its Receptor Protein Kinase Regulate Plant Cell Expansion. Science *343*, 408–411. https://doi.org/10.1126/science.1244454.
39. Kuroda, R., Kato, M., Tsuge, T., and Aoyama, T. (2021). Arabidopsis phosphatidylinositol 4-phosphate 5-kinase genes PIP5K7, PIP5K8, and PIP5K9 are redundantly involved in root growth adaptation to osmotic stress. The Plant Journal *106*, 913–927. https://doi.org/10.1111/tpj.15207.
40. Feng, W., Kita, D., Peaucelle, A., Cartwright, H.N., Doan, V., Duan, Q., Liu, M.-C., Maman, J., Steinhorst, L., Schmitz-Thom, I., et al. (2018). The FERONIA Receptor Kinase

Maintains Cell-Wall Integrity during Salt Stress through Ca2+ Signaling. Current Biology, 1–31. https://doi.org/10.1016/j.cub.2018.01.023.
41. Jaillais, Y., Bayer, E., Bergmann, D.C., Botella, M.A., Boutté, Y., Bozkurt, T.O., Caillaud, M.-C., Germain, V., Grossmann, G., Heilmann, I., et al. (2024). Guidelines for naming and studying plasma membrane domains in plants. Nat. Plants *10*, 1172–1183. https://doi.org/10.1038/s41477-024-01742-8.
42. Noack, L.C., Bayle, V., Armengot, L., Rozier, F., Mamode-Cassim, A., Stevens, F.D., Caillaud, M.-C., Munnik, T., Mongrand, S., Pleskot, R., et al. (2022). A nanodomain-anchored scaffolding complex is required for the function and localization of phosphatidylinositol 4-kinase alpha in plants. The Plant Cell *34*, 302–332. https://doi.org/10.1093/plcell/koab135.
43. Fratini, M., Krishnamoorthy, P., Stenzel, I., Riechmann, M., Matzner, M., Bacia, K., Heilmann, M., and Heilmann, I. (2021). Plasma membrane nano-organization specifies phosphoinositide effects on Rho-GTPases and actin dynamics in tobacco pollen tubes. The Plant Cell *33*, 642–670. https://doi.org/10.1093/plcell/koaa035.
44. Zhao, C., Zayed, O., Yu, Z., Jiang, W., Zhu, P., Hsu, C.-C., Zhang, L., Tao, W.A., Lozano-Durán, R., and Zhu, J.-K. (2018). Leucine-rich repeat extensin proteins regulate plant salt tolerance in Arabidopsis. Proceedings of the National Academy of Sciences of the United States of America *4*, 201816991.
45. Chen, J., Xu, F., Qiang, X., Liu, H., Wang, L., Jiang, L., Li, C., Wang, B., Luan, S., Wu, D., et al. (2024). Regulated cleavage and translocation of FERONIA control immunity in Arabidopsis roots. Nat. Plants, 1–14. https://doi.org/10.1038/s41477-024-01823-8.
46. Ischebeck, T., Werner, S., Krishnamoorthy, P., Lerche, J., Meijon, M., Stenzel, I., Lofke, C., Wiessner, T., Im, Y.J., Perera, I.Y., et al. (2013). Phosphatidylinositol 4,5-Bisphosphate Influences PIN Polarization by Controlling Clathrin-Mediated Membrane Trafficking in Arabidopsis. THE PLANT CELL ONLINE.
47. Lebecq, A., Doumane, M., Fangain, A., Bayle, V., Leong, J.X., Rozier, F., Marques-Bueno, M. del, Armengot, L., Boisseau, R., Simon, M.L., et al. (2022). The Arabidopsis SAC9 enzyme is enriched in a cortical population of early endosomes and restricts PI(4,5)P2 at the plasma membrane. eLife *11*, e73837. https://doi.org/10.7554/eLife.73837.
48. Doumane, M., Lebecq, A., Colin, L., Fangain, A., Stevens, F.D., Bareille, J., Hamant, O., Belkhadir, Y., Munnik, T., Jaillais, Y., et al. (2021). Inducible depletion of PI(4,5)P2 by the synthetic iDePP system in Arabidopsis. Nature Plants, 1–24. https://doi.org/10.1038/s41477-021-00907-z.
49. Johnson, A., Gnyliukh, N., Kaufmann, W.A., Narasimhan, M., Vert, G., Bednarek, S.Y., and Friml, J. (2020). Experimental toolbox for quantitative evaluation of clathrin-mediated endocytosis in the plant model Arabidopsis. Journal of Cell Science *133*, jcs248062. https://doi.org/10.1242/jcs.248062.
50. Chen, W., Zhou, H., Xu, F., Yu, M., Coego, A., Rodriguez, L., Lu, Y., Xie, Q., Fu, Q., Chen, J., et al. (2023). CAR modulates plasma membrane nano-organization and immune signaling downstream of RALF1-FERONIA signaling pathway. New Phytologist *n/a*. https://doi.org/10.1111/nph.18687.
51. Menzel, W., Stenzel, I., Helbig, L.-M., Krishnamoorthy, P., Neumann, S., Eschen-Lippold, L., Heilmann, M., Lee, J., and Heilmann, I. (2019). A PAMP-triggered MAPK cascade inhibits phosphatidylinositol 4,5-bisphosphate production by PIP5K6 in Arabidopsis thaliana. New Phytologist *224*, 833–847. https://doi.org/10.1111/nph.16069.
52. Xu, J., and Scheres, B. (2005). Dissection of Arabidopsis ADP-RIBOSYLATION FACTOR 1 function in epidermal cell polarity. THE PLANT CELL *17*, 525–536.

53. Stuttmann, J., Barthel, K., Martin, P., Ordon, J., Erickson, J.L., Herr, R., Ferik, F., Kretschmer, C., Berner, T., Keilwagen, J., et al. (2021). Highly efficient multiplex editing: One-shot generation of 8x Nicotiana benthamiana and 12x Arabidopsis mutants. The Plant journal : for cell and molecular biology.
54. Gökaltun, A., Kang, Y.B. (Abraham), Yarmush, M.L., Usta, O.B., and Asatekin, A. (2019). Simple Surface Modification of Poly(dimethylsiloxane) via Surface Segregating Smart Polymers for Biomicrofluidics. Sci Rep *9*, 7377. https://doi.org/10.1038/s41598-019-43625-5.
55. von Wangenheim, D., Hauschild, R., Fendrych, M., Barone, V., Benková, E., and Friml, J. (2017). Live tracking of moving samples in confocal microscopy for vertically grown roots. eLife *6*, e26792. https://doi.org/10.7554/eLife.26792.
56. Schindelin, J., Arganda-Carreras, I., Frise, E., Kaynig, V., Longair, M., Pietzsch, T., Preibisch, S., Rueden, C., Saalfeld, S., Schmid, B., et al. (2012). Fiji: an open-source platform for biological-image analysis. Nat Methods *9*, 676–682. https://doi.org/10.1038/nmeth.2019.
57. Pylvänäinen, J.W., Laine, R.F., Saraiva, B.M.S., Ghimire, S., Follain, G., Henriques, R., and Jacquemet, G. (2023). Fast4DReg – fast registration of 4D microscopy datasets. J Cell Sci *136*, jcs260728. https://doi.org/10.1242/jcs.260728.
58. Chiu, C.-L., Clack, N., and the napari community (2022). napari: a Python Multi-Dimensional Image Viewer Platform for the Research Community. Microanal *28*, 1576–1577. https://doi.org/10.1017/S1431927622006328.

Key resources table

REAGENT or RESOURCE	SOURCE	IDENTIFIER
Bacterial and virus strains		
Escherichia coli DH5-α	Thermo Scientific™	EC0112
Biological samples		
Plasmid pDGE332-M1	10.1111/tpj.15197	Addgene#153241
Plasmid pDGE333-M2	10.1111/tpj.15197	Addgene#153242
Plasmid pDGE335-M3	10.1111/tpj.15197	Addgene#153244
Plasmid pDGE337-M4E	10.1111/tpj.15197	Addgene#153246
Plasmid pDGE651	10.1111/tpj.15197	Addgene#153229
Chemicals, peptides, and recombinant proteins		
Murashige and Skoog basal medium	Duchefa	M0221
Propidium iodide	Sigma-Aldrich	P4864
FM4-64	Life Technologies	T-3166
PDMS-PEG	Cymit Quimica	3H-DBE-712
PDMS Sylgard 184	Farnell	101697
SU-8 2050 photoresist resin	MicroChem	
Fluorescein Dextran 10 kDa	Invitrogen	D1821
RAFL23 peptide	10.1093/plphys/kiab308	Synthetized by Proteogenix
RALF1 peptide	10.1093/plphys/kiab308	Synthetized by Proteogenix
Experimental models: Organisms/strains		
Arabidopsis thaliana: Columbia-0 ecotype, wild type	NASC	Col-0
Arabidopsis thaliana: pip5k7,8,9 in Col-0 background	10.1111/tpj.14932	na
Arabidopsis thaliana: Col-0/mcitrine-2PH(EVECTIN)	10.1016/j.devcel.2018.04.011	na
Arabidopsis thaliana: Col-0/mcitrine-1PH(FAPP1)	10.1111/tpj.12358	na
Arabidopsis thaliana: Col-0/mcitrine-1PH(OSBP)	10.1111/tpj.12358	na
Arabidopsis thaliana: Col-0/mcitrine-2PH(PLC)	10.1111/tpj.12358	na
Arabidopsis thaliana: feronia in Col-0 background/mcitrine-2PH(PLC)	created for this manuscript	na
Arabidopsis thaliana: Col-0/mcitrine-1PH(PLC)	10.1111/tpj.12358	na
Arabidopsis thaliana: pip5k7,8,9 in Col-0 background/mcitrine-1PH(PLC)	10.1111/tpj.15207	na
Arabidopsis thaliana: Col-0/mcitrine-TUBBYc	10.1111/tpj.12358	na
Arabidopsis thaliana: Col-0/PIP5K7-YFP	10.1111/tpj.15207	na
Arabidopsis thaliana: Col-0/PIP5K8-YFP	10.1111/tpj.15207	na

Arabidopsis thaliana: Col-0/PIP5K9-YFP	10.1111/tpj.15207	na
Arabidopsis thaliana: Col-0/PIN2-GFP		na
Arabidopsis thaliana: pip5k7,8,9 in Col-0 background/PIN2-GFP	10.1111/tpj.15207	na
Oligonucleotides		
FERONIA_Guide1_Forward	TTGATCGATGAAGATCACAG	na
FERONIA_Guide2_Forward	TACACTTTCCCTGTAGCATC	na
FERONIA_Guide3_Forward	TCTATTGGATGAGAAATGGG	na
FERONIA_Guide4_Forward	ATCGTTGATCCCTACCTCAA	na
Software and algorithms		
ImageJ/FIJI	https://imagej.net/software/fiji/	1.54p
Python Anaconda	https://www.anaconda.com/	Python 3.12.10/Anaconda 25.3.1
LRC	https://github.com/NBCS1/LRCv2	v2

Materials & Methods:

1. Biological material and growth conditions

In all the experiments, the *Arabidopsis thaliana* (*A. thaliana*) accession Columbia-0 (Col-0) was used as the wild type and as a genetic background. The following lines were published before: *pip5k7,9*, *pip5k7,8,9*, 2PH(PLC), 1PH(PLC), 1PH(FAPP1), 1PH(OSBP), 1TUBBYc, 2PH(EVECTIN), PIN2::PIN2-GFP, PIP5K7::PIP5K7-YFP, PIP5K8::PIP5K8-YFP, PIP5K9::PIP5K9-YFP.[26,27,30,39,52]

Seeds were surface sterilized using chlorine gas, vernalized at 4°C for 2 days and grown on solid (0.8%, Agar plant, Duchefa) quarter-strength Murashige and Skoog media supplemented with 1% sucrose at pH 5.8 for 5 days at 21°C in a 16-h light/8-h dark cycle with 70% relative humidity and a light intensity of 200 µmol photons.m-2.s-1 prior experiment.

2. CRISPR-Cas9 mutation of FERONIA

Four CRISPR guides directed against both FERONIA intracellular and extracellular spaces were selected using the website https://chopchop.cbu.uib.no/ (**Figure S3**).

The plasmid for transformation were prepared using the CRISPR-Cas9 cloning system and protocol developed in [53]. *A. thaliana* lines expressing either mCITRINE-2PH(PLC) or mCITRINE-1PH(FAPP1) biosensors were transformed using *Agrobacterium tumefaciens* floral dipping.

3. Microfluidic chips fabrication and microfluidic flow system

Microfluidics chips were created by modifying the design from Serre et al., 2021.[19] Chips were manufactured by UV-Photolithography using SU-8 2050 photoresist resin (MicroChem) spinned at 1750 rpm on 10cm diameter wafers in order to obtain 90µm channel height.

Chips were then molded in PDMS Sylgard 184 at a 15:5 ratio to obtain a stickier polymer. One publication suggested that RALFs peptides bind and saturate PDMS chips.[18] To limit this phenomenon we added 2% PDMS-PEG copolymer block (Cymit Quimica, 3H-DBE-712) in the PDMS mix to increase hydrophilicity and reduce potential peptide binding.[54]

Microfluidic experiments were carried out using manually closable microfluidic chips (as described in [19]). Briefly, 5-day-old seedlings were transferred onto an open microfluidic chip containing two root channels pre-filled with ¼ MS, pH 5.8, 1% sucrose and 7µg/ml propidium iodide (Sigma-Aldrich, P4864). The chips were then manually closed with a coverslip before applying a constant flow of medium. Seedlings were let to recover from the transfer vertically on the microscope for 20 minutes before imaging. Imaging consisted of 3 frames spaced by 2 minutes in control condition (¼ MS, pH 5.8, 1% sucrose) then 18 frames (36 minutes) in treatment condition (¼ MS, pH 5.8, 1% sucrose + treatment). Arrival of the treatment was followed with a background fluorophore added in different concentrations in both media (Fluorescein Dextran 10 kDa, Invitrogen™, D1821).
The microfluidic system and chips were thoroughly washed with isopropanol and mQ water after each use to avoid RALF contaminations. A stable 3 µL per minute flow control was obtained using the OB1 pressure controller and MFS2 thermal flow sensors from Elveflow (Elvesys group, France). We added four Shape-memory alloy valves (Memetis group, Germany) in the flow path setup as two 1 x input / 2 x outputs valves. In this configuration, we prevented media backflow and assured that media were constantly flowing either toward a trash or toward the chip, preventing excessive RALF peptide sticking to the tubing and unmoving medium close to the heating element of the thermal flow sensors (see **Figure S1C**).

4. Microscopic imaging

All microscopic observations were carried out on an LSM 980 Axio Observer 7 (Carl Zeiss group, http://www.zeiss.com/) equipped with an AiryScan 2 module and GaAsP-PMT detectors. The microscope body is set up as a vertical stage microscope to keep seedlings in their natural orientation.[55]
Experiments conducted in microfluidics were imaged in Airyscan Multiplex mode using a 20x objective (Plan-Apochromat 20x/0.8 M27) for confocal imaging.
FM4-64, PIP5K7-YFP and PIN2-GFP experiments were visualized in Airyscan super-resolution mode with a 40x objective (C-Plan-Apochromat 40x/1,30).

5. FM4-64 and PIN2-GFP internalization assays

To assess the endocytosis process, we performed FM4-64 internalization assay following a protocol described in Johnson *et al. 2020*.[49] Seedlings were incubated in liquid ¼ MS medium, 1% sucrose, containing 0 or 5µM RALF23 for 10 minutes then transferred to corresponding media supplemented with 2 µM FM4-64 for 10 minutes. Seedlings were then washed twice and mounted between slide and coverslip in their respective media without FM4-64 for immediate imaging.
For the observations of PIN2-GFP internalization, seedlings were incubated in liquid ¼ MS medium, 1% sucrose, containing 0 or 5µM RALF23 for 10 minutes and then mounted between slide and coverslip in their respective media

6. Image analysis and quantifications

LRC image processing pipeline:

Imaging of seedlings expressing anionic phospholipid biosensors was done along with the imaging of the same tissues stained with propidium iodide used as a cell contour reference. Seedlings were imaged over time every 2 minutes allowing to image two seedlings and make seven Z slices per frame. These Z slices allowed to not lose the original focus on the cell of interest as some treatment can induce shrinking and swelling of the tissues and thus, Z shifts.

Using 4D registration of the movies, we are able to follow the same group of cells from t_0 to t_{end} with minimal shift in Z.
After a preprocessing phase consisting of preparing the raw data for registration, the FIJI[56] plugin Fast4D reg[57] was ran in batch mode to register in time and space the movies using the propidium iodide channel as a reference to apply to the biosensor channel which can change signal over time and treatments. Next, the only manual step of the pipeline was the manual selection of the region of interest (ROI) (**Figure S1C**). This step is assisted by using the Napari image viewer[58] and a dedicated interface.
Then, following a determined segmentation protocol (**Figure S1C**), the cell contours and intracellular signal mask are created automatically for each cell over time (**Figure 1B**). We implemented functions to check the identity (in space) of the cells compared to the previously detected ones in order to be able to follow one cell over a whole experiment.
We used a background fluorescent tracer with different concentration in the control and treatment media allowing to quantify the arrival of the treatment (see 2.). After a manual roi selection in the background, the treatment arrival frame was automatically determined and applied to the time columns.
The intracellular and plasma membrane masks were used to quantify the average fluorescence in each compartment for each cell of each seedling over time. Fluorescence values were then used to create the ratio plasma membrane fluorescence/Intracellular fluorescence.
In microfluidic data were normalized to obtain control values starting around a ratio of 1. The normalization was obtained by dividing each time point for a given replicate by its average ratio (plasma membrane fluorescence/Intracellular fluorescence) in control between time -6 and -2 minutes before treatment. The normalized data was called association index in this manuscript.

FM4-64 and PIN2-GFP internalization quantification:
For FM4-64 and PIN2-GFP internalization and quantification of intracellular compartment density or sizes, we used a modified version of LRC segmentation module to obtain individual cell intracellular masks that were used to segment individual intracellular compartments. Individual Intracellular compartment characteristics were retrieve using the measure.regionprops_table function from the scikit-image Python package.
For FM4-64 tonoplast staining percentages, cell presenting tonoplast staining were manually assessed over the overall cell number visible in each image.

PIP5K7-YFP cluster quantification:
PIP5K7-YFP cluster size and density were obtain by manual ROI selections and global fixed-value thresholding of intracellular compartment. Individual intracellular compartment characteristics were retrieve using the measure.regionprops_table function from the scikit-image Python package.

7. Plotting and statistical analysis:

All plots shown in this manuscript were obtain using the Python Seaborn package (https://doi.org/10.21105/joss.03021.).
All statistics conducted in this manuscript were non-parametric tests from the Python Scipy.stats package. For comparison of two conditions or genotypes we used two-sided Mann-Whitney U tests. For multi comparisons of different conditions/genotypes to the control

condition/genotype, we first used a Kruskal-Wallis test followed by two-sided Mann-Whitney U tests. Each test and the p-values obtained are available in supplementary file statistics.

Data and scripts availability:

The latest version of the LipidRatioCalculator (LRC) program developed for this publication is available at https://github.com/NBCS1/LRCv2.

The Python scripts used to quantify the density or size of intracellular compartments in the FM4-64 and PIN2-GFP internalization assays can be found at https://github.com/NBCS1/FERONIA-RALFs-Phosphoinositides-paper_scripts.

All preprocessed microscopy data will be deposited on Zenodo or similar platforms for publication.

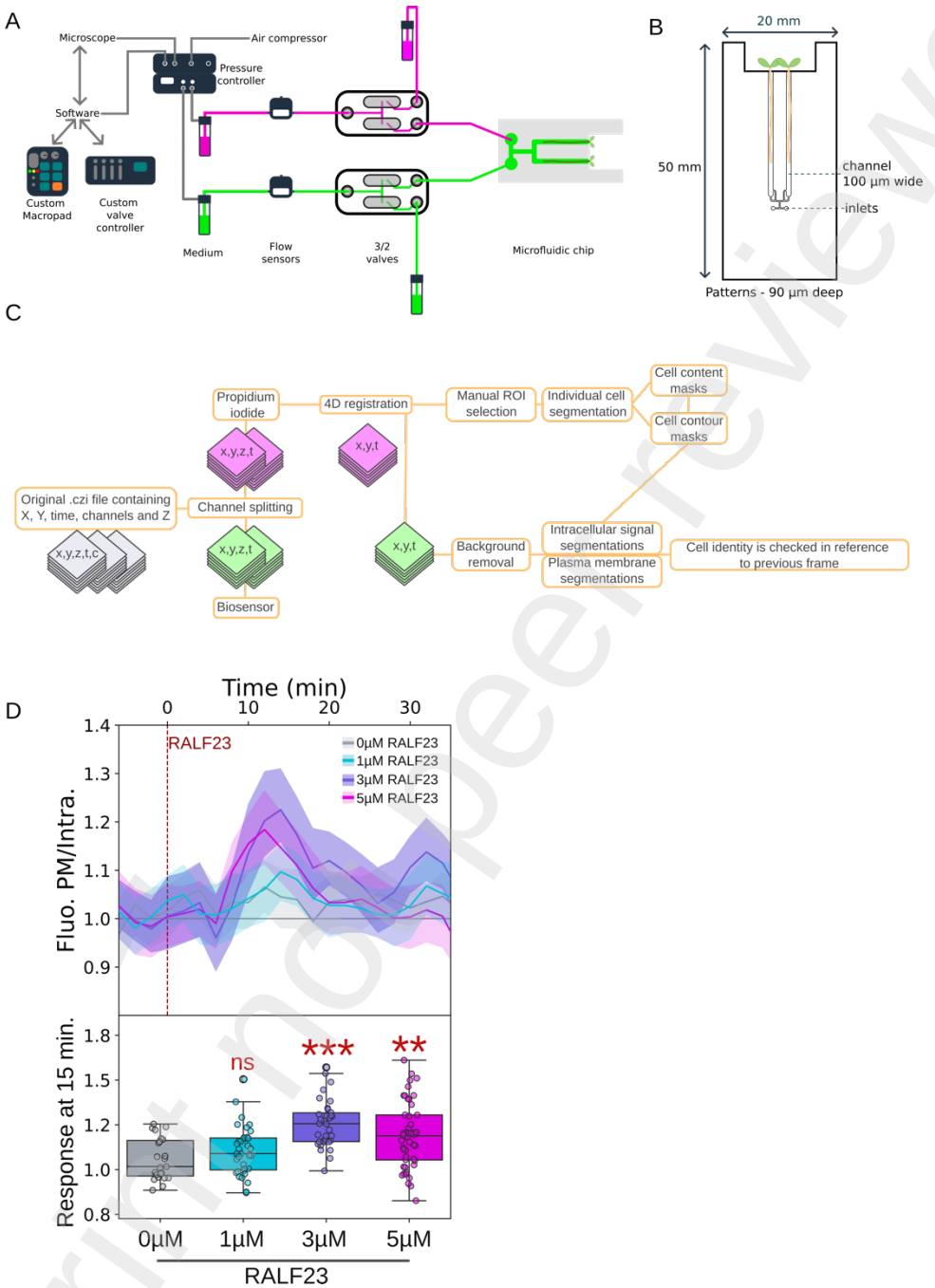

Figure S1 (related to Figure 1): Schematic representation of the microfluidic system and image analysis pipeline used in this study. A*) Overview of the microfluidic system used in this publication. A more detailed description is available in materials and methods.* ***B****) Close-up schematic of the microfluidic chip used in this study.* ***C****) Schematic representing the sequential steps carried out by the semi-automated image analysis program.* ***D****) Upper panel: Quantification of the mCITRINE-2PH(EVECTIN) association index over time (minutes) in response to a gradient of RALF23 (0, 1, 3, 5 µM RALF23). Lower panel: Box plots showing the distribution of association index values in individual cells at 15 minutes, for control (0 µM RALF23) and treated (0, 1, 3, 5 µM RALF23) conditions. n cells [23-48] from [8-11] individual seedlings. p-value 0 vs 1µM = 0.1716 (p > 0.05: ns), 0 vs 3µM = 5.05e^{-06} (p < 0.001: ***), 0 vs 5µM = 0.0048 (p < 0.01: **). Note that the data for the control and 5 µM condition are the same than in figure 1.*

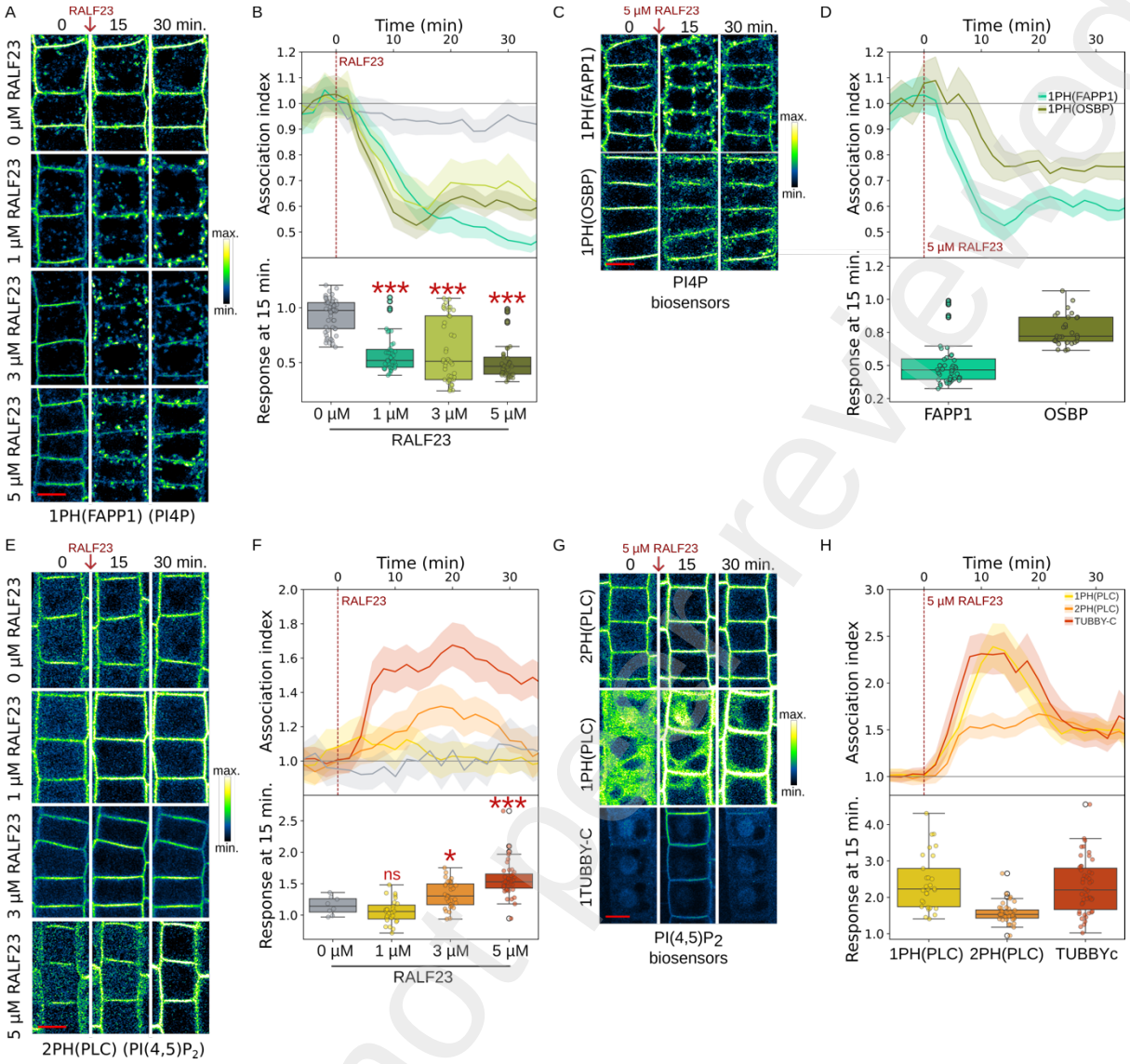

Figure S2 (related to Figure 2): RALF23 dose-dependent response of PI4P and PI(4,5)P_2 biosensors. A,E*) Representative microscopy images of A) PI4P biosensor mCITRINE-1PH(FAPP1) and E) PI(4,5)P_2 biosensor mCITRINE-2PH(PLC) imaged in microfluidic. Seedlings were imaged in control condition (t0) and then in treatment condition 0, 1, 3 or 5 µM RALF23 (t15 and t30). Scale bar = 10 µm.* ***B,F****) Upper panel: Quantification of the B) mCITRINE-1PH(FAPP1) and F) mCITRINE-2PH(PLC) association index over time (minutes). Lower panel: Box plots showing the distribution of association index values in individual cells at 15 minutes, for control (0 µM RALF23) and treated (1, 3 or 5 µM RALF23) conditions. For B) n cells [42-52] from [7-9] individual seedlings and F) n cells [8-40] from [4-8] individual seedlings. p-values are detailed in Supplementary file (p < 0.001: ***).* ***C,G****) Representative microscopy images of A) PI4P biosensors mCITRINE-1PH(FAPP1), mCITRINE-1PH(OSBP) and G) PI(4,5)P_2 biosensors mCITRINE-2PH(PLC), mCITRINE-1PH(PLC) and mCITRINE-1TUBBYc imaged in microfluidic. Seedlings were imaged in control condition (t0) and then in treatment condition 5 µM RALF23 (t15 and t30). Scale bar = 10 µm.* ***D,H****) Upper panel: Quantification of the B) mCITRINE-1PH(FAPP1) and F) mCITRINE-2PH(PLC) association index over time (minutes). Lower panel: Box plots showing the distribution of association index values in individual cells at 15 minutes after treatment with 5 µM RALF23. For D) n cells [29-44] from [5-8] individual seedlings and H) n cells [29-46] from [5-9] individual seedlings. Note that the data for the control and 5 µM condition are the same than in figure 2.*

Figure S3 (related to Figure 3): Characterization of CRISPR-mediated mutation in FERONIA. *Genomic DNA alignment of FERONIA genomic DNA and sequencing results obtained in feronia CRISPR-Cas9 mutants obtained in plant expressing the 2PH(PLC) or the 1PH(FAPP1) anionic phospholipid biosensors. Guide RNA used are indicated in yellow. Insertion in green and deletion in magenta. Guide 1 and 2 are targeting FERONIA extracellular domain while guide 3 and 4, the intracellular domain.*

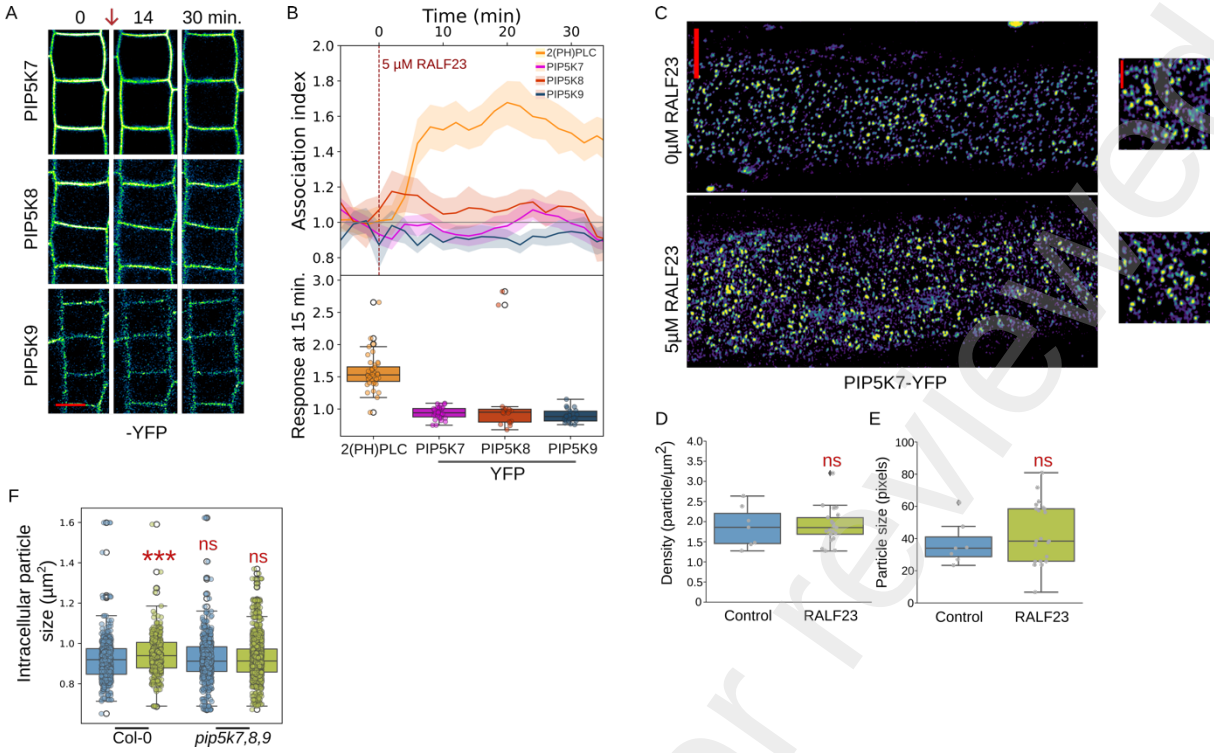

Figure S4 (related to Figure 4): PIP5K7/8/9 localization is not perturbed upon RALF23 treatment. ***A****) Representative microscopy images in microfluidics of PIP5K7-YFP, PIP5K8-YFP and PIP5K9-YFP. Seedlings were imaged in control condition (t0) and then in treatment with 5 µM RALF23 (t15 and t30). Scale bar = 10 µm.* ***B****) Upper panel: Quantification of PIP5K7-YFP, PIP5K8-YFP and PIP5K9-YFP association indexes over time (minutes) in response to 5 µM RALF1. Lower panel: Box plots showing the distribution of association index values in individual cells at 15 minutes treated with 5 µM RALF1. n cells [17-40] from [3-8] individual seedlings.* ***C****) Representative microscopy images of PIP5K7-YFP plasma membrane clusters. Seedlings were imaged after treatment with 0 or 5 µM RALF23 (t15 and t30). Scale bar = 10 µm. Quantification of PIP5K7-YFP plasma membrane clusters in control and treatment with 5 µM RALF23:* ***D)*** *density and* ***E)*** *size. p-values are detailed in Supplementary file (p>0,05: non significant (ns)). [7-21] individual seedlings.* ***F****) Quantification of the size of intracellular fluorescent particles after FM4-64 internalization assays and treatment with 0 or 5 µM RALF23. [22-35] individual seedlings. p-values are detailed in Supplementary file (p>0,05: non significant (ns), p < 0.001: ***).*

Video S1: Timelapse obtained in microfluidics with the PI4P sensors indicated at the top. The arrival of RALF23 treatment is indicated by the orange square. Images are taken every two minutes.

Video S2: Timelapse obtained in microfluidics with the PI(4,5)P_2 sensors indicated at the top. The arrival of RALF23 treatment is indicated by the orange square. Images are taken every two minutes.

Video S1: Timelapse obtained in microfluidics with the PI(4,5)P_2 sensor mCITRINE-1PH(PLC) in the wild type and *pip5k7,8,9* triple mutant. The arrival of RALF23 treatment is indicated by the orange square. Images are taken every two minutes.